Annals of Biomedical Engineering, Vol. 39, No. 2, February 2011 *(© 2010)* pp. 850–863
DOI: 10.1007/s10439-010-0200-6

Intracranial Stents Being Modeled as a Porous Medium: Flow Simulation in Stented Cerebral Aneurysms

L. AUGSBURGER,[1,2] P. REYMOND,[1] D. A. RUFENACHT,[3] and N. STERGIOPULOS[1]

[1]Laboratory of Hemodynamics and Cardiovascular Technology, School of Life Science, École Polytechnique Fédérale de Lausanne, CH-1015 Lausanne, Switzerland; [2]Neuro-Interventional Service, Clinical Neurosciences Department, University Hospital of Geneva, Geneva, Switzerland; and [3]Department of Neuroradiology, Swiss Neuro Institute, Hirslanden Klinic, Zurich, Switzerland

(Received 10 March 2010; accepted 20 October 2010; published online 2 November 2010)

Associate Editor Aleksander S. Popel oversaw the review of this article.

Abstract—Intracranial aneurysms may be treated by flow diverters, alternatively to stents and coils combination. Numerical simulation allows the assessment of the complex nature of aneurismal flow. Endovascular devices present a rather dense and fine strut network, increasing the complexity of the meshing. We propose an alternative strategy, which is based on the modeling of the device as a porous medium. Two patient-specific aneurysm data sets were reconstructed using conventional clinical setups. The aneurysms selection was done so that intra-aneurismal flow was shear driven in one and inertia driven in the other. Stents and their porous medium analog were positioned at the aneurysm neck. Physiological flow and standard boundary conditions were applied. The comparison between both approaches was done by analyzing the velocity, vorticity, and shear rate magnitudes inside the aneurysm as well as the wall shear stress (WSS) at the aneurysm surface. Simulations without device were also computed. The average flow reduction reaches 76 and 41% for the shear and inertia driven flow models, respectively. When comparing the two approaches, results show a remarkable similarity in the flow patterns and magnitude. WSS, iso-velocity surfaces and velocity on a trans-sectional plane are in fairly good agreement. The root mean squared error on the investigated parameters reaches 20% for aneurysm velocity, 30.6% for aneurysm shear rate, and 47.4% for aneurysm vorticity. It reaches 20.6% for WSS computed on the aneurysm surface. The advantages of this approach reside in its facility to implement and in the gain in computational time. Results predicted by the porous medium approach compare well with the real stent geometry model and allow predicting the main effects of the device on intra-aneurismal flow, facilitating thus the analysis.

Keywords—Cerebral aneurysm, Computational fluid dynamics, Flow simulation, Intracranial stent, Porous medium.

INTRODUCTION

Intracranial aneurysms are pathological dilatations of an artery that may rupture under certain circumstances. Aneurysm rupture is followed by subarachnoid hemorrhage (SAH) which presents high morbidity and mortality rates for the patients concerned.[32] A majority of aneurysms is found on bifurcations at or in the vicinity of the circle of Willis.[11] A clinical study reports that about 2% of the population is carrying such intracranial aneurysm, whereas the rupture incidence has been estimated to reach about 9 over 100,000 individuals (0.01%) each year in western countries.[28] Co-factors recognized to contribute to intracranial aneurysm growth and rupture have been widely investigated.[6,27,31]

Endovascular treatment of unruptured intracranial aneurysms results in better clinical outcomes when compared to traditional surgery.[22] Coils have been widely used for the treatment of aneurysms. Coils are long metallic preshaped wires that are delivered inside the aneurysm allowing filling the cavity, and stabilizing the disease. However, other studies reveal that using bare platinum coils, only 55% of aneurysms can completely be obliterated, 24% are partially treated while in 18%, a treatment cannot be achieved.[32] A recent study emphasizes also that the recanalization rate of an aneurysm following coil embolization is found higher in ruptured and aneurysms having a diameter of more than 8 mm, or in young patients.[23]

Contrary to the stents commonly used to treat stenoses, intracranial stents have been developed to support coils packed in the aneurismal cavity. Stents are flexible, self-expanding porous tubular meshes made of stainless steel or other alloys such as Nitinol. *Stent-in-stent* techniques which do not require the use of coils

Address correspondence to L. Augsburger, Laboratory of Hemodynamics and Cardiovascular Technology, School of Life Science, École Polytechnique Fédérale de Lausanne, CH-1015 Lausanne, Switzerland. Electronic mail: luca.augsburger@epfl.ch

anymore in dissecting or small wide-necked aneurysms have been reported.[3,4,15,33] Such *stent-in-stent* configuration results in an increased lateral hemodynamical resistance thereby reducing intra-aneurysmal flow.

Flow diverters differ from intracranial stents and are characterized by very thin wires (30–50 μm), very small windows or pores (~100 μm) and a single or a multilayer structure. Their design is consequently very different when compared with conventional stents. These devices can be braided or laser-cut, and are optimized to facilitate aneurysm occlusion in a stand-alone mode. As flow diverters are exhibiting smaller cell design, their placement and position in regard with the aneurismal neck is no longer an issue. Studies reveal the porosity of such devices to be the major parameter that drives their ability to impede or modify the aneurismal flow.[16,18] However, when considering a potential and inadvertent blockage of perforating vessels, their porosity cannot be too low ($<65\%$). Tests including flow diverters have been reported.[2,14] Recently, Sadasivan *et al*. compared the efficiency of various flow diverters in elastase-induced aneurysms in rabbits and reported that the pore density rather than porosity alone may be a critical factor for device efficacy modulation.[26]

Blood flow simulation in intracranial aneurysms has become the method of choice for assessing aneurismal flow. Indeed, as flow is currently thought to be a key factor in the understanding of aneurysm growth and rupture, a correct assessment of flow patterns and related quantities, such as wall shear stress (WSS) can help clinicians in a personalized evaluation of a specific aneurysm rupture risk. These hemodynamic quantities and their derivates such as oscillatory shear index, positive WSS gradient have been implicated in aneurysm growth and rupture.[5,8,19,20,30]

The effect of intracranial stents on aneurysm hemodynamics can be predicted by numerical techniques, such as computational fluids dynamics (CFD). Among others, Aenis *et al*. simulated the effect of an idealized stent in an idealized model of sidewall aneurysm,[1] whereas Cebral and Lohner developed an efficient method allowing for quantifying cerebral aneurysms hemodynamics changes using an adaptive embedding technique.[7] The large difference of scale between the size of the flow diverters' struts and the aneurysm (up to 30 mm) creates difficulties in the mesh process and flow diverters are consequently more difficult to simulate using conventional methods, because of the higher number of elements created and higher need of computational power.

In this study, we propose to simulate the effects of one flow diverter using CFD based on porous medium approach in two patient-specific intracranial aneurysm geometries. The advantage of simulating the flow diverter as a porous medium consists in reducing the number of elements and therefore the computational power. Simulation results are then compared with the real stent simulation.

METHODS

Anatomical models

The first patient (Case A) had no previous history of SAH. He was diagnosed in 2003 with a SAH. A ruptured sidewall aneurysm was found in the left internal cerebral artery. The second patient (Case B) was diagnosed in 2004 with a SAH. A ruptured intracranial aneurysm found on the bifurcation of the anterior communicating artery was found. An illustration of the aneurysm shape for both aneurysms is shown in Fig. 1. Data sets of the two models were acquired with a three-dimensional subtraction angiography (Philips Health Care, Best, the Netherlands) and were further reconstructed in a 512^3 resolution matrix.

The choice of the geometries was done to have a case of a shear driven flow (Case A) and an inertia driven flow (Case B). Indeed, the interest resides in the fact that these flows behave in a complete different manner from a fluid mechanics point of view. In the first geometry, the aneurysm flow is created by friction from the parent artery flow. In this kind of configuration, low exchange of blood between the parent artery and the aneurysm cavity is observed. In the second geometry, the parent artery flow points directly into the aneurysm. The flow hits the aneurysm dome directly creating intense fluidic exchange between the parent artery and the aneurysm. Simulation without endovascular device were also computed in order to calculate the flow reduction factors.

The morphological parameters of the two selected aneurysms are shown in Table 1. Values are given in millimeters.

Stent

The intracranial stent model was based on the SILK Stent (Balt International, Montmorency, France). This endovascular device is a stent made of nitinol with a dense strut network designed for the redirection of flow. It is composed by 48 wires; 40 wires have a diameter of 30 μm and 8 have a diameter of 50 μm. An illustration of the device in its straight configuration is shown in Fig. 2 (left). Rhinoceros 4.0 (Seattle, WA, USA) was used to bend and fit the device in the aneurysm neck. For sake of computational power, only the stent struts placed in the aneurismal neck were kept, whereas the struts lodged against the artery wall were cropped and excluded from the simulation.

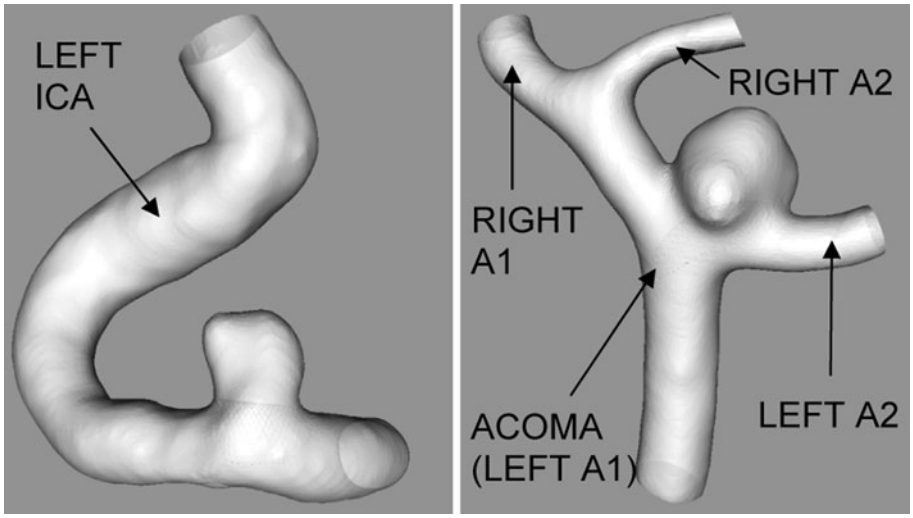

FIGURE 1. Illustration of two geometries simulated: the shear driven flow model (left) and the inertia driven flow model (right).

TABLE 1. Morphological characterization of case A (shear driven) and case B (inertia driven) aneurysms.

	Case A Shear driven	Case B Inertia driven
Aneurysm		
Height	5.93	5.07
Width	6.50	5.08
Depth	5.99	7.71
Artery		
Height	5.76	3.17
Width	6.83	4.18
Neck		
Length	5.32	5.74
Width	6.37	4.56

The aneurysm height corresponds to the maximum distance between the neck center and the aneurysm dome. The aneurysm width is the maximum distance measured on the aneurysm wall perpendicularly to the flow direction. The aneurysm depth is the maximum distance measured on the aneurysm's wall in parallel to the flow direction. The artery height is the diameter of the artery as measured in its cross section in the direction of the aneurysm, whereas the artery width is measured perpendicularly to the artery height. The neck length is measured in the direction of the flow, whereas the neck width is measured perpendicularly.

Illustrations of the stented aneurysms models are shown in Fig. 2 (middle and right).

Porous Medium

The porous medium is modeled by the addition of a momentum source term to the standard fluid flow equations. It is composed of a viscous loss term and an inertial loss term. This momentum sink contributes to the pressure gradient across the porous cells, creating a pressure drop that is proportional to the fluid velocity. In our case, we assumed a simple homogeneous porous medium, for which the momentum sink becomes

$$S_i = -\left(\frac{\mu}{\alpha}v_i + C_2\frac{1}{2}\rho|v|v_i\right), \tag{1}$$

where i is the ith (x, y, or z) coordinate, $|v|$ is the magnitude of the velocity, α is the permeability, C_2 is the inertial resistance factor, μ is the viscosity, and ρ is the density. Thus, the methodology presented here

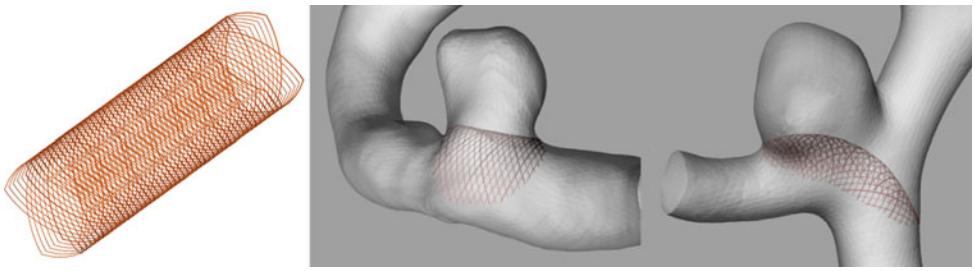

FIGURE 2. Illustration of the SILK stent in its straight configuration (left) and in the two simulated models (middle and right).

requires the specification of the inverse permeability α^{-1} and the inertial resistance factor C_2 for flow through the porous medium. These coefficients can be obtained either experimentally or via numerical simulations. We chose to perform CFD simulations, where we computed the relationship between pressure drop and velocity through the porous component. These simulations were done in a *long* pipe, having a cross section of 1 mm^2 (1.128 mm of diameter) and in a *long* rectangular parallelepiped, presenting a cross section of 0.18 mm^2 (0.9 mm per 0.2 mm). A plate section of the stent—similar as the screens defined in Kim *et al.*[17]—was reproduced and introduced in the test volumes. As the stent exhibits a non-homogenous design and in order to model the perpendicular and the tangential porous medium coefficients, the stent was placed in the long pipe perpendicularly to the flow direction (Fig. 3a) and in the long rectangular parallelepiped in parallel to the flow direction (Fig. 3b), respectively.

The pressure drop is expressed as a function of blood velocity as a second order polynomial of the form

$$\Delta p = av^2 + bv \tag{2}$$

was fitted to the data, where Δp is the pressure drop and v is the velocity. A simplified form of the momentum equation, relating the pressure drop to the source term, can be expressed as

$$\Delta p = -S_i \Delta e, \tag{3}$$

where Δe is the porous medium thickness. Combining Eqs. (1), (2), and (3), we obtain $a = C_2 \frac{1}{2} \rho \Delta e$ and $b = \frac{\mu}{\alpha} \Delta e$. The coefficients of the inverse permeability α^{-1} and the drag factor C_2 are consequently equal to

$$C_2 = \frac{2a}{\rho \Delta e} \quad \text{and} \quad \alpha = \frac{\mu}{b} \Delta e$$

Two sets of coefficients are thus obtained for a stent placed perpendicularly and parallel to the flow.

Effect of a Non-Planar Geometry

The volume representing the flow diverter is delimited by non-planar surfaces, which are bended and consequently not aligned with global coordinates. For each point in the porous medium, we had to define the normal and the tangential direction of the local porous medium characteristics, as these are defined from the numerical simulation when the stent was placed perpendicularly and parallel to the flow. The coefficients are scalars and pertain to the local normal and tangential directions of the porous medium surface. Once these local directions are defined, the solver assigns the porous medium coefficients to the adjacent tetrahedral finite volume elements. Hence, if the stent surface is curved, as is in the general case, the porous medium coefficients vary locally.

Mesh

The meshing was performed using ICEM CFD 11.0 (Ansys Inc., Canonsburg, PA, USA). For the models with a flow diverter, an adaptive mesh approach was preferred. Mesh smoothing was applied using Ansys inherent smoothing routines. The number of elements, as well as mean and minimal mesh factor quality

TABLE 2. Number of elements, mean and minimal mesh quality factor for the two aneurysms, the two approaches and for the unstented cases.

Approach	Number of cells	Mean mesh quality	Min. mesh quality
Case A: shear driven flow model			
Stent	7,426,366	0.73	0.34
Porous medium	777,051	0.73	0.17
Unstented	957,304	0.73	0.36
Case B: inertia driven flow model			
Stent	8,850,897	0.71	0.30
Porous medium	586,412	0.74	0.16
Unstented	1,202,620	0.73	0.41

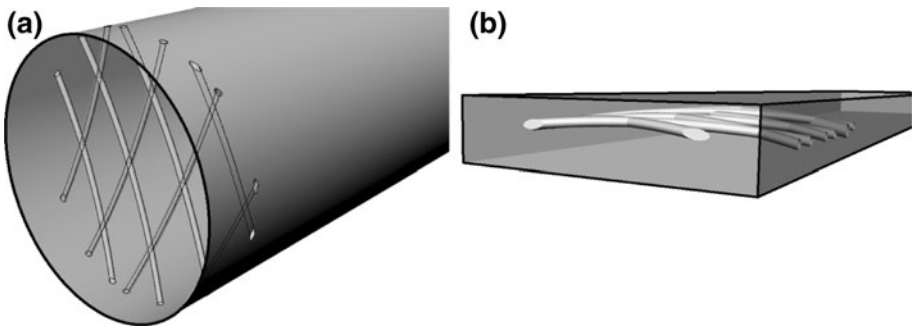

FIGURE 3. (a, b) Perpendicular (left) and parallel (right) placement of the stent in the test sections.

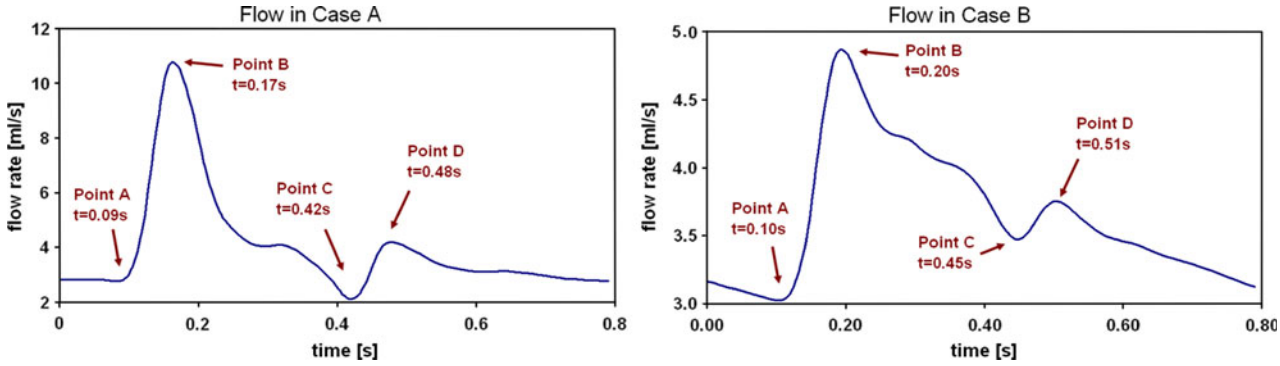

FIGURE 4. Illustration of the flow rate curves applied at the inlet of Case A and Case B.

reached is shown in Table 2. The mesh quality is given by the computation of the deformation of the elements in the mesh by first calculating the Jacobian of each hexahedron and then normalizing the determinant of the matrix. A value of 1 represents a perfect hexahedral cube, while a value of −1 is a totally inverted cube with a negative volume. Mesh dependency tests were performed in order to ensure the stability of the simulations.

TABLE 3. Main flow parameters for the applied flow rate curves in Cases A and B.

Parameter	Units	Case A	Case B
$RE_{min}/RE_{max}/RE_{mean}$	–	54/273/102	141/226/170
$Q_{min}/Q_{max}/Q_{mean}$	mL/s	2.11/10.72/4.00	3.03/4.86/3.64
$V_{min}/V_{max}/V_{mean}$	cm/s	6.13/31.15/11.64	29.43/47.25/35.42
α	–	4.78	2.61
Pulsatility index	–	2.15	0.50

Flow

Blood flow measurements were not available for the two patient's cases. Therefore, in order to set boundary conditions as physiological as possible, flow rate waveforms were computed using a generic one-dimensional (1-D) model described in Reymond *et al.*[25] The 1-D form of the fluid equations was applied over each arterial segment. A non-linear viscoelastic constitutive law for the arterial wall was considered. The arterial tree dimensions and properties were taken from the literature and completed with real patient scans and coupled to a model of the left ventricle based on the varying elastance.

This generic 1-D model has been validated qualitatively with averaged *in vivo* measurements performed on different persons. Pressure was measured with applanation tonometry and cerebral blood flow velocities with transcranial ultrasound and phase contrast MRI. The main systemic arteries were modeled, including as well, a detailed description of the cerebral circulation. Pressure and flow waveforms were then available at each location of the arterial tree. We represented in Fig. 4, the generic flow rate curves simulated for Cases A and B.

Points A, B, C, and D indicate the four comparison points between the real flow diverter simulated and the results given by a porous medium approach.

The main flow parameters are summarized in Table 3. Q_{mean} represents the mean flow rate given in milliliters per second (mL s^{-1}); V_{mean} is the mean velocity in centimeters per second (cm s^{-1}). The Womersley number, α, is a dimensionless number which expresses the ratio of inertia effects due to pulsating flow to viscous effects and it is defined by $\alpha = r(\omega\rho\mu^{-1})^{0.5}$, where r is the parent artery internal radius, ω is the angular frequency, and μ is the dynamic viscosity. Finally, the pulsatility index is given by $(V_{max} - V_{min})/V_{mean}$, where V_{max} and V_{min} are the maximal and minimal flow velocity during the cardiac cycle, respectively.

Simulation

Blood flow was simulated using Fluent 6.0 (Ansys, Canonsburg, PA, 15317). Blood was modeled as an incompressible Newtonian fluid with a density of 1.06 g cm^{-3} and a viscosity of 4 mPa s. Vessel walls were assumed to be rigid with a no slip boundary condition at the walls. The outlet flow was set in order to set a physiological WSS at the outlets. We imposed the same mean shear stress in the outlets, which with the local geometry allowed us to obtain the mean flow rates in the outlets. Hence, we have the distribution of flow in the exit branches, which is what the solver requires.

The unsteady flow was computed with a time step of 0.01 s for a cardiac cycle period of $T = 0.8$ s. In each simulation, three cardiac cycles were computed and the third cardiac cycle only was taken for the analysis. The flow rate as shown in Fig. 3 was approximated by its

Fourier transformation using the first ten harmonics. A fully developed flow, as obtained by the Womersley solution for the input flow was imposed as boundary condition at the inflow plane.

Postprocessing

Postprocessing was performed using Paraview 3.4 (opensource, www.paraview.org). For the quantification of differences between the two approaches, calculations were performed using custom made routines on Matlab 7.7.0.471 (The Mathworks, Natick, MA, USA).

TABLE 4. Comparison of flow velocity, vorticity, and shear rate without device, with porous medium and with the real stent; the reduction factors are given in parenthesis.

	Without device	Porous medium	Stent
Shear driven flow			
Velocity (mm/s) (%)			
Mean	24.55	5.05 (79.4)	6.245 (74.5)
Max	191.52	63.90 (66.6)	67.55 (64.7)
Vorticity (mPa) (%)			
Mean	169.59	36.71 (78.3)	35.85 (79.8)
Max	962.34	222.27 (76.9)	194.77 (80.3)
Shear rate (s^{-1}) (%)			
Mean	0.31	0.06 (79.8)	0.06 (80.3)
Max	4.05	1.26 (68.8)	0.72 (82.3)
Inertia driven flow			
Velocity (mm/s) (%)			
Mean	85.58	29.31 (65.8)	25.6 (70.01)
Max	498.62	332.02 (33.4)	298.20 (40.2)
Vorticity (mPa) (%)			
Mean	1048.59	237.00 (77.4)	400.66 (61.79)
Max	6270.61	3347.89 (46.6)	7552.75 (−20.44)
Shear rate (s^{-1}) (%)			
Mean	1.95	0.54 (72.1)	0.66 (66.0)
Max	23.29	23.90 (−2.6)	28.27 (−21.38)

RESULTS

Comparison of the Flow Reduction in the Presence of a Flow Diverter

Table 4 shows the comparison of flow velocity, vorticity, and shear rate without device, with porous medium, and with the real stent. The mean velocity reduction reaches 71.3% in the shear driven flow model and 52.4% in the inertia driven flow model. The vorticity reduction reaches 78.8 and 41.3% in the shear and inertia driven flow models, respectively. The shear rate reduction reaches 77.8 and 28.5% in the shear and inertia driven flow models, respectively.

Characterization of Porous Medium

The pressure drop versus a range of imposed velocities is shown in Figs. 5a and 5b for the stent placed perpendicularly and in parallel to the flow direction, respectively. The drop of pressure is approximated to

$$\Delta p = 367.08 \cdot V^2 + 281.35 \cdot V \quad \text{with} \quad R^2 = 0.9992 \quad \text{and}$$

$$\Delta p = 1452 \cdot V^2 + 4188 \cdot V \quad \text{with} \quad R^2 = 1$$

for the stent placed perpendicularly and in parallel to flow direction, respectively.

The viscous resistance and inertial resistance coefficients derived from the above numerical simulations are shown in Table 5.

Qualitative Comparison of Intra-Aneurismal Flow Characteristics

In Figs. 6 and 7, we illustrate blood flow in the stented aneurysm models, the flow diverter being modeled as a real flow diverter (top) and as a porous

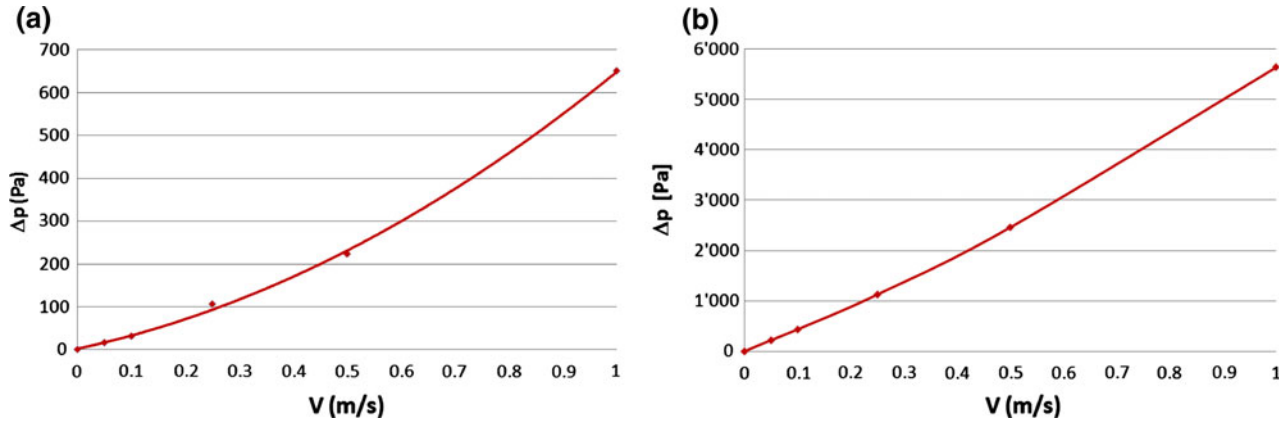

FIGURE 5. Relation between pressure drop and imposed velocity for a sample of the SILK stent placed (a) perpendicularly to the flow direction in a 1 mm^2 cylindrical cross section, and (b) parallel to the flow direction in a rectangular parallelepiped having a cross section of 0.9 × 0.2 mm.

TABLE 5. Flow diverters' viscous inertial resistance and inertial resistance factors adapted for the two geometries.

Porous medium parameters	Viscous resistancelinear $1/\alpha$ ($1/m^2$)		Inertial resistance Quadratic C_2 (1/m)	
	Tangential	Normal	Tangential	Normal
Shear and inertia driven flow models	1.7*E*9	8.9*E*8	4′697	8′703

medium (bottom). The first part illustrates the flow in the shear driven flow model (Case A), whereas the second illustrates the flow in the inertia driven flow model (Case B). Points A, B, C, and D correspond to the four points in the cardiac cycle shown in Fig. 4. Figures 6a, 6b, 6c, and 6d, illustrate the results of the simulation for the shear driven flow (Case A). Iso-velocity surfaces, velocity magnitude on a plane, and WSS are compared, respectively. Figure 7a, 7b, 7c, 7d, and 7e illustrate the results of the simulation for the inertia driven flow (Case B). Iso-velocity surfaces, velocity magnitude on a plane, and WSS are compared.

The general qualitative observation is that the two approaches are presenting very comparable results. The iso-velocity surfaces are found to be extremely similar. Surface size, shapes, orientations, and directions are corresponding well for all four points of the cardiac cycle, for both the shear driven and inertia driven flow models. The velocity magnitude depicted on the selected plane is coherent within the two approaches. Inflow, outflow, and recirculation zones are similar. In Fig. 7b, the flow diverter approach illustrates perfectly the geometry of the flow diverter, where blood flow is observed to pass through the flow diverters' pores, creating locally higher velocity magnitudes. Naturally, such flow features, placed closed to the flow diverter are not completely reproduced by the porous medium approach. Elsewhere, however, the velocity magnitude in the aneurysm as well as in the parent arteries is found to be similar.

Furthermore, WSS patterns are similar in shape and magnitude. Small differences can be reported, especially at the neck of the aneurysm, where the WSS patterns are found somehow smoother in the porous medium approach as compared to those simulated with the real flow diverter. However, regions of low or high WSS are matching perfectly, in location and size. WSS patterns at the aneurysm dome are also matching very well.

Quantitative Comparison

In order to allow for a quantitative comparison between the real stent and the porous medium approach, we plotted, for the shear driven flow model, the mean and maximum values of the velocity, the vorticity, and the shear rate within the aneurysm as a function of time for one cardiac cycle time (Fig. 9a). Figure 9b compares the averaged value of mean and maximum WSS value at the entire aneurysm surface (first column), the aneurysm dome (second column), and the aneurysm neck (third column). Figure 8 put in evidence the aneurysm dome and neck regions for the shear (left) and for the inertia (right) driven flow models. The same comparison is proposed in Figs. 9c, and 9d for the inertia driven flow model.

The graphs are presenting similar patterns. Especially for the shear driven flow, all quantities match very well except for the maximum shear rate, which is somewhat overestimated. In the case of inertia driven flow, the patterns are still overall good, but the porous medium approach tends to underestimate velocity and vorticity, especially during systole.

Table 6 summarizes the root mean square values (in parenthesis the error in %) of the mean and maximum values of velocity, shear rate, and vorticity computed in the aneurysm, as well as the mean and maximum WSS computed on the entire aneurysm surface, aneurysm dome and neck surfaces, averaged over one cardiac cycle.

The mean error for velocity reached 26.8% for the shear driven flow and 13.15% for the inertia driven flow model. The mean error for shear rate computed inside the aneurysm reached 42.4% for the shear driven flow model and 18.89% for the inertia driven flow model. The mean error for vorticity reached 45% for the shear driven flow model and 49.86% in the inertia driven flow model. The mean error for WSS reaches 18.6% on the aneurysm surface, 89.3% on the aneurysm dome, and 19.5% on the aneurysm neck in the shear driven flow model. The mean error for WSS reaches 22.52% on the aneurysm surface, 44.06% on the aneurysm dome, and 15.9% on the aneurysm neck in the inertia driven flow model.

The parameter presenting the largest error is the maximum WSS computed at the dome of the aneurysm, in the shear driven flow model (97.4%). Without considering this value, the error on WSS would reach 31.5% only. The second value presenting the largest difference when compared to the real stent approach is the mean WSS computed on the aneurysm dome (81.2%), in the shear driven model. The parameters presenting the smallest difference are the maximum velocity computed in the inertia driven flow model

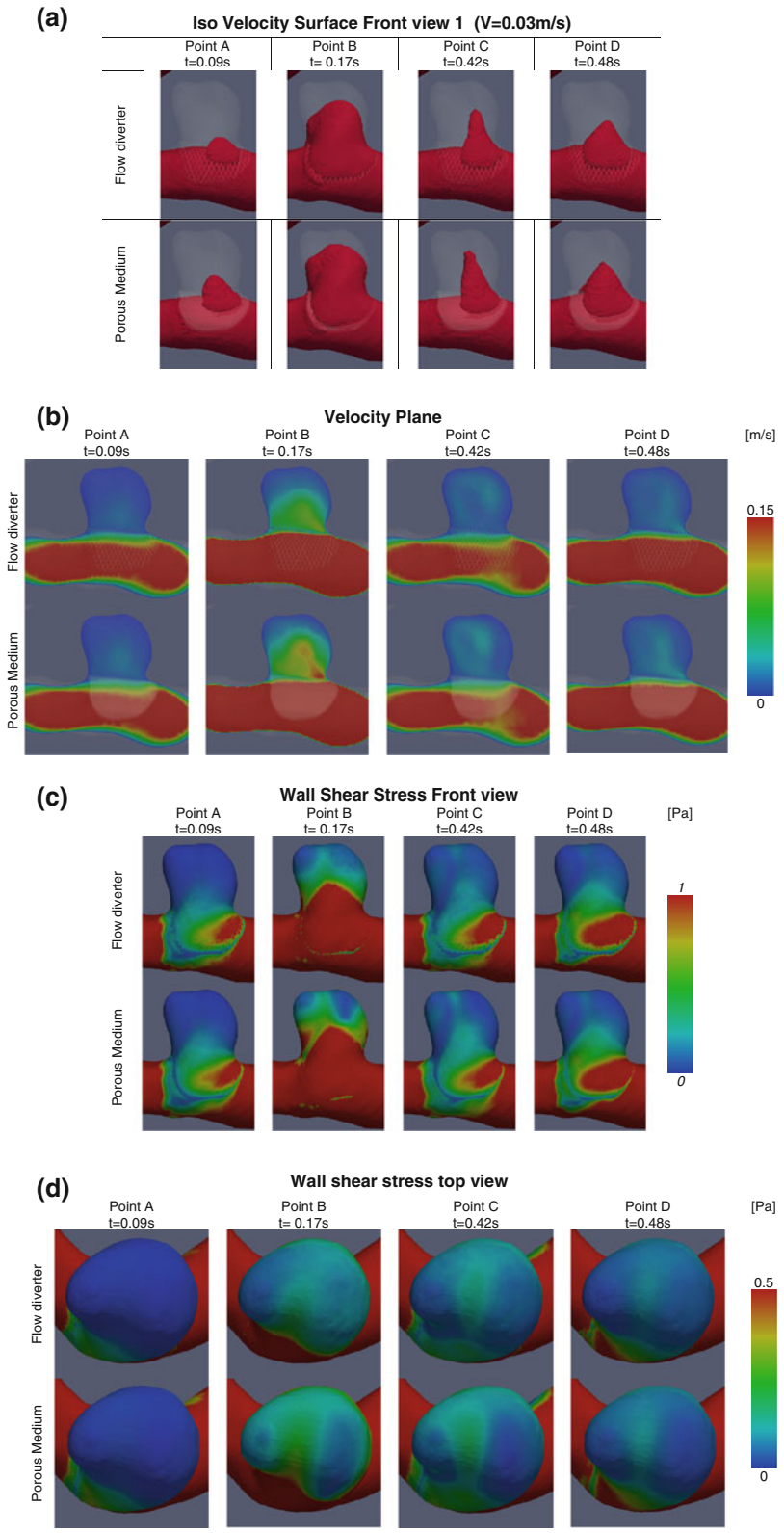

FIGURE 6. Shear driven flow model. (a) Flow represented as an iso-velocity surface for the flow diverter (top) and the porous medium (bottom) at the four cardiac cycle points. (b) Velocity magnitude in a plane at the four cardiac cycle points. (c) Wall shear stress at the four cardiac cycle points. (d) Wall shear stress at the four cardiac cycle points.

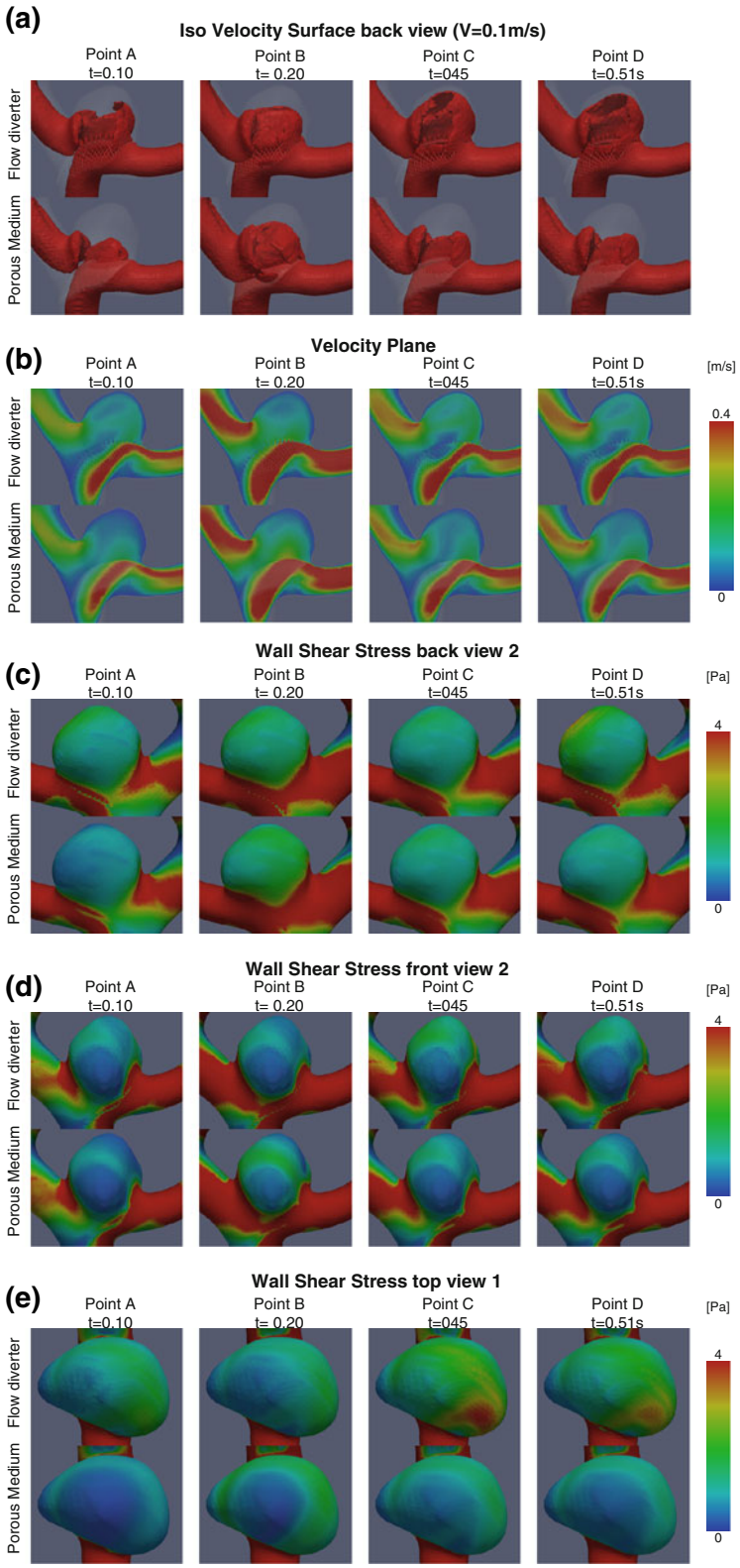

FIGURE 7. Inertia driven flow model. (a) Flow represented as an iso-velocity surface for the flow diverter (top) and the porous medium (bottom) at the four cardiac cycle points. (b) Velocity magnitude in a plane at the four cardiac cycle points. (c) Wall shear stress at the four cardiac cycle points. (d) Wall shear stress at the four cardiac cycle points. (e) Wall shear stress at the four cardiac cycle points.

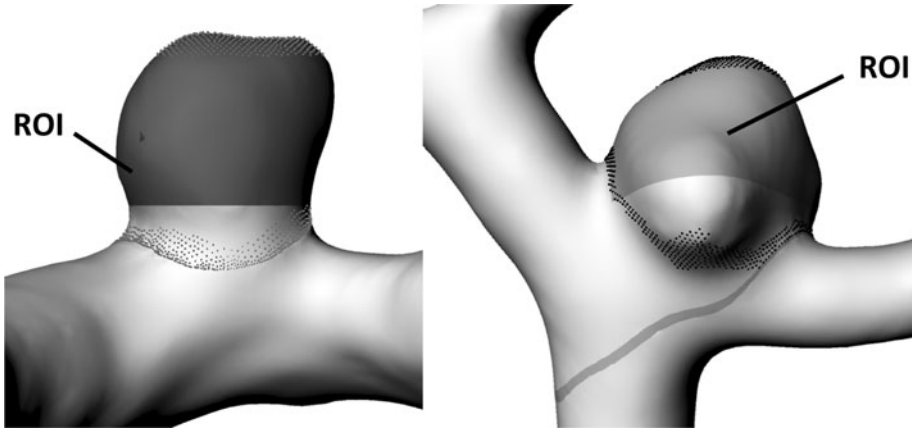

FIGURE 8. Regions of interest (ROI) where quantitative comparison is done, for the shear (left) and for the inertia (right) driven flow models. ROI represents the volume of the aneurysms where velocity, vorticity, and shear rate are compared. The dots represent the locations on the aneurysms dome and neck surfaces, where wall shear stresses are compared.

(6.77%), and the WSS computed at the neck of the aneurysm (11.09%), in the inertia driven model.

DISCUSSION

We sought an alternative strategy for computing, using CFD, the complex interactions between flow diverters and local blood flow in intracranial aneurysms. As flow diverters have dense networks of very thin struts, the mesh required for precise and stable CFD simulations of the real stent contains typically one order of magnitude more nodes that a typical mesh in the absence of stent. This renders the computation difficult and lengthy. Our approach was to replace the stent with a porous medium, with the appropriate resistances in the tangential and normal to stent directions. These endovascular devices are usually not considered for ruptured aneurysms, however, we aimed at testing this approximate modeling approach in two patient-specific aneurysm geometries, representing a shear driven and an inertia driven flow. The results are quite encouraging, in the sense that the qualitative features of intra-aneurismal flow are well captured and the errors in absolute values are reasonable.

Previously, a porous medium approach was used to assess hemodynamic changes in coiled aneurysms.[9,12,13,21] Such models were developed to understand the probability of aneurysm recanalization. Kim *et al*. calculated hydraulic resistances of two commercial stents,[17] whereas Walliez and Coussement quantified changes in blood flow due to the insertion of a multi-layer stent in abdominal aortic aneurysms.[29] The only report that presents a fully two-dimensional theoretical model using a porous medium based approach was done by Fernandez *et al*.[10] and it was applied to the Lylyk© stent in idealized and patient-specific aneurysm models. Unfortunately, the authors did not compare the results of the porous medium approach with the real stent geometry.

The simulation shows similarities in the iso-velocity surfaces, WSS patterns and velocity on a transsectional plane between the porous medium and the flow diverter in both shear and inertia driven aneurysms at four different timesteps of the cardiac cycle. Such similarities could also be observed at the acceleration phase (i.e., at $t = 0.15$ s). When comparing the graphs of the aneurysm velocity, vorticity, and shear rate, a clear correspondence is observed in the shear driven case, the wave shapes are almost identical and the absolute values compare with acceptable levels of error for the complexity of the system. The analysis of the WSS computed on the aneurysm, dome, and neck surfaces is also showing resemblance between both approaches. The porous medium approach seems, however, in some cases to underestimate the investigated values, especially at systole and in the inertia driven flow aneurysm.

The principal interest of this method consists in the reduced number of elements, which in our case is a factor 12 in reduction. This makes meshing process easier and faster, without the need of excessive computational power. Also, the reduced time of calculation is estimated to reach a factor 20 and allows to predict the efficiency of a given flow diverter in a given patient-specific aneurysm with a satisfying precision within a reasonable clinical time, typically within 4–6 h. The range of errors found between the porous medium and the real stent simulations where in the same order of magnitude as between different simulations of a stented aneurysm performed by different numerical techniques during the First Virtual Intracranial Stenting Challenge.[24]

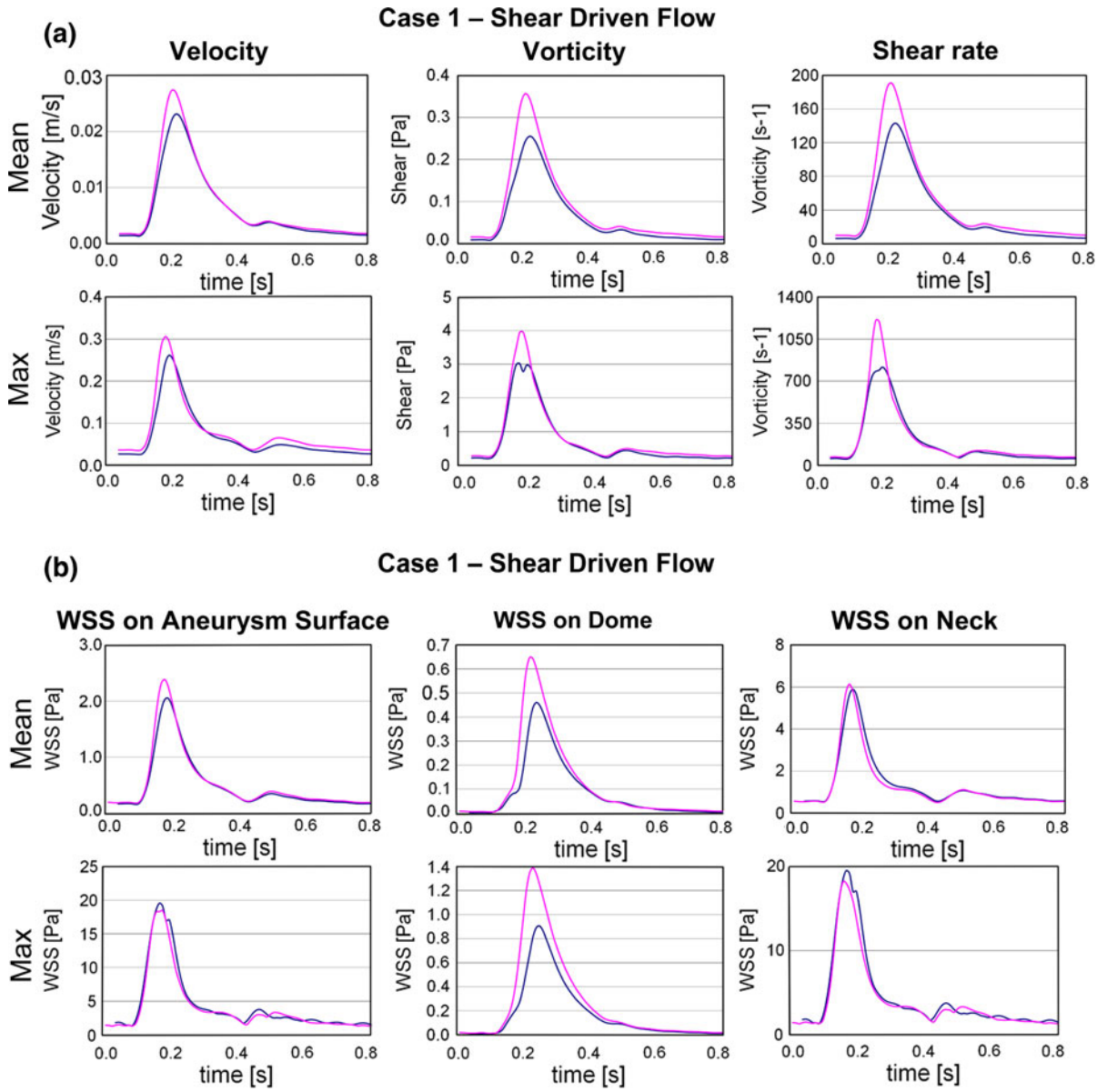

FIGURE 9. (a) Mean and maximum values of velocity, vorticity, and shear rate computed in the aneurysm, in the shear driven flow model (blue line = real stent; magenta line = porous medium). (b) Mean and maximum values of wall shear stress, computed on the aneurysm surface, dome and neck, in the shear driven flow model (blue line = real stent; magenta line = porous medium). (c) Mean and maximum values of velocity, vorticity, and shear rate computed in the aneurysm, in the inertia driven flow model (blue line = real stent; magenta line = porous medium). (d) Mean and maximum values of wall shear stress, computed on the aneurysm surface, dome and neck, in the inertia driven flow model (blue line = real stent; magenta line = porous medium).

The successful modelization of a flow diverter as a porous medium does not seem to be dependant on the aneurysms configuration or any kind of flow. In our case, the results were better for the shear driven flow model. This may derive from the fact that in the shear driven flow, the bulk of flow entry into to the aneurismal space comes from a direction parallel to the stent surface. The apparent porosity is larger and likely the assessment of the porous medium properties more precise in this case. In inertia driven flows, there is a very strong interaction of the flow running perpendicularly to the stent plane with the stent struts and this may lead to high sensitivity of the effective porosity on the particular spatial disposition of the stent with respect to the adjacent flow. There is no general rule on how to choose the porosity coefficients for any general stent. These coefficients should be adapted for each specific stent that is been studied since the porous medium coefficients needs to be adapted for each particular stent geometry. Ideally, one could study parametrically different stent geometries, represented by some key geometrical characteristics (i.e., strut size,

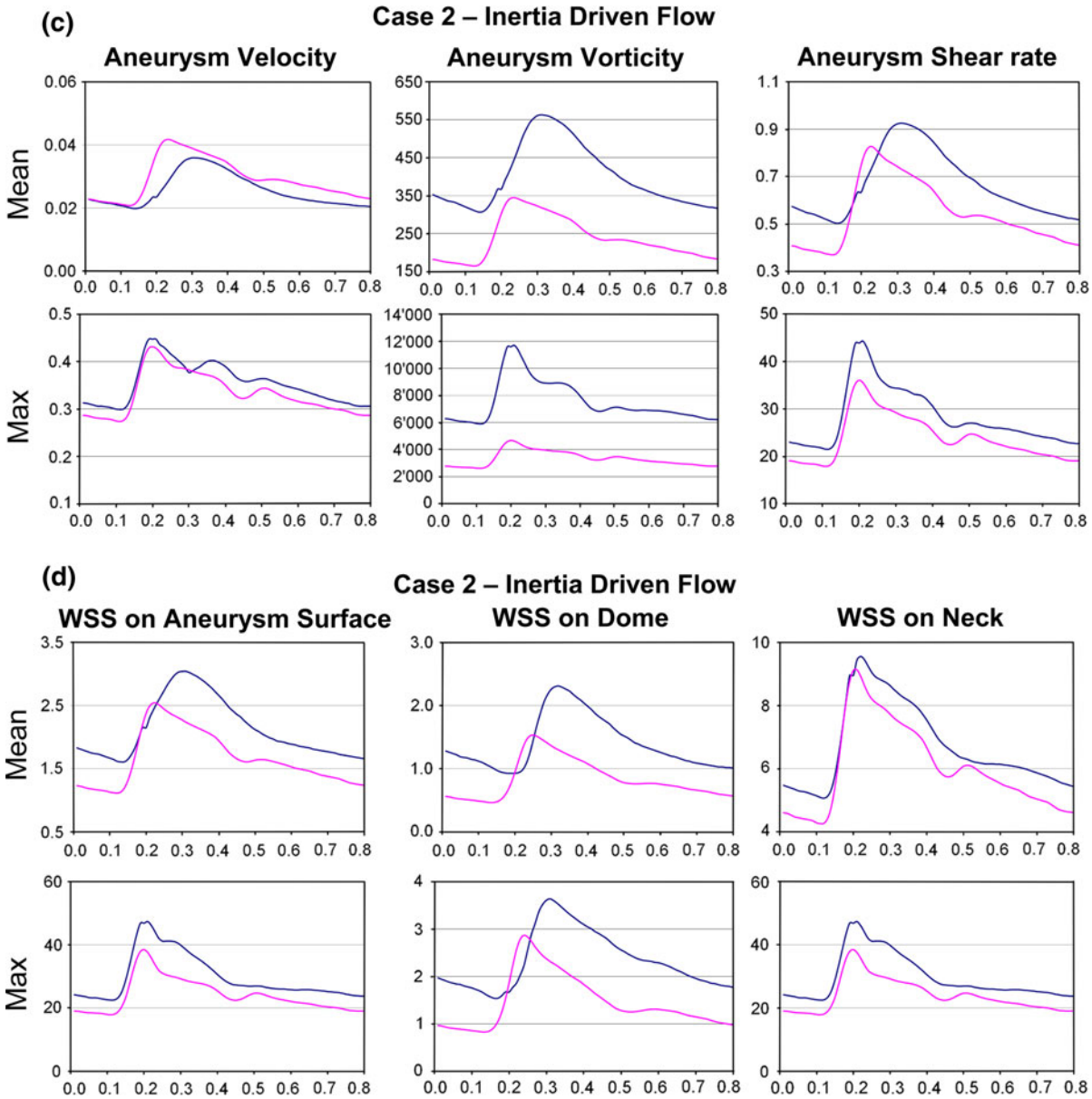

FIGURE 9. Continued.

cell size, porosity, *etc.*) and different flow angles of attack and try to derive empirical relations linking porous media coefficients to stent design and local flow characteristics. Such a comprehensive study should be envisioned in some future work. Also, the reason to change the test geometry (circular and rectangular box) is due to the fact that if placed parallel to the flow within the circular cylinder, we obtained very small pressure drops. Hence, we preferred to confine the stent within a narrow parallelepiped to obtain more significant pressure drops, which make the parameter identification a bit easier.

In these simulations, the velocity is found to be low at the aneurysm neck after stenting. However, the quadratic term in Eq. (2) remains of importance since this approach is intended to be used in any patient-specific aneurysm geometry, especially in terminal aneurysms as found in the basilar artery where the velocity at the aneurysm neck may remain significant after stenting.

Also, the exact positioning of the stent would require a much more comprehensive approach which would include the interaction of the self-expanding stent and the elastic wall. We think, however, that even if the exact positioning of the stent is not captured by our approach using Rhinoceros, the fluidic effects of the stent are well represented, and especially the comparison with the porous medium model, which follows the exact same geometry and positioning of the stent, is still valid.

TABLE 6. Absolute root mean square of the error (RMSE) and its relative value in % (divided by the average of the mean and maximum values) of the investigated parameters.

Inside RMSE (relative RMSE)	Velocity (mm/s) (%)	Shear rate (mPa) (%)	Vorticity (s^{-1}) (%)
Shear driven flow			
Mean	1.44 (23.1)	33.17 (54.7)	16.65 (46.5)
Max	20.62 (30.5)	215.08 (30.1)	84.81 (43.5)
Inertia driven flow			
Mean	5.00 (19.54)	142.55 (21.47)	170.22 (42.48)
Max	24.01 (6.77)	4602.01 (16.28)	4322.33 (57.23)

WSS surface RMS (RMS-E)	Aneurysm (mPa) (%)	Dome (mPa) (%)	Neck (mPa) (%)
Shear driven flow			
Mean	106.81 (21.5)	72.97 (81.2)	281.35 (20.4)
Max	704.98 (15.8)	179.52 (97.4)	829.85 (18.6)
Inertia driven flow			
Mean	517.63 (24.33)	641.32 (45.72)	743.68 (11.09)
Max	61614 (20.7)	991.60 (42.41)	61614.5 (20.7)

Numerical simulation of blood flow in intracranial aneurysms is based on various assumptions. We assumed rigid walls, blood is modeled as a Newtonian fluid and the boundary conditions are taken from 1D models. As raised by Fernandez *et al.*, in 2008[10] it could be questionable to claim that one solves the flow through an endovascular device having a strut size of 30 μm while neglecting the red blood cells size having a size of about 8 μm which occupy about 50% of the blood volume. Consequently, numerical simulations, even those of the CFD on the real stent geometry, are rather a rough representation of reality. In that respect and considering the logical levels of the differences resulting from both approaches, the porous medium maybe a preferred approach, because it yields faithful reproductions of most qualitative and to some extend quantitative features of intra-aneurismal flow. We conclude that the porous medium approach is of interest for the prediction of flow diverter efficiency. The need to identify better the viscous and inertial resistance values for a proper modeling of a flow diverter is to be considered in future experiments.

ACKNOWLEDGMENTS

This work was generated in the framework of the @neurIST Project, which is co-financed by the European Commission through the contract no. IST-027703. This work has also been partially supported by StrokeLab Inc., Geneva, Switzerland.

REFERENCES

[1]Aenis, M., *et al*. Modeling of flow in a straight stented and nonstented side wall aneurysm model. *J. Biomech. Eng*. 119(2):206–212, 1997.
[2]Ahlhelm, F., *et al*. Treatment of wide-necked intracranial aneurysms with a novel self-expanding two-zonal endovascular stent device. *Neuroradiology* 49(12):1023–1028, 2007.
[3]Ahn, J. Y., *et al*. Endovascular treatment of intracranial vertebral artery dissections with stent placement or stent-assisted coiling. *AJNR Am. J. Neuroradiol*. 27(7):1514–1520, 2006.
[4]Benndorf, G., *et al*. Treatment of a ruptured dissecting vertebral artery aneurysm with double stent placement: case report. *AJNR Am. J. Neuroradiol*. 22(10):1844–1848, 2001.
[5]Burleson, A. C., and V. T. Turitto. Identification of quantifiable hemodynamic factors in the assessment of cerebral aneurysm behavior. On behalf of the Subcommittee on Biorheology of the Scientific and Standardization Committee of the ISTH. *Thromb. Haemost*. 76(1):118–123, 1996.
[6]Cannon Albright, L. A., *et al*. A genealogical assessment of heritable predisposition to aneurysms. *J. Neurosurg*. 99(4): 637–643, 2003.
[7]Cebral, J. R., and R. Lohner. Efficient simulation of blood flow past complex endovascular devices using an adaptive embedding technique. *IEEE Trans. Med. Imaging* 24(4): 468–476, 2005.
[8]Cebral, J. R., *et al*. Cerebral aneurysm hemodynamics modeling from 3D rotational angiography. In: Proc. 2004 IEEE International Symposium on Biomedical Imaging: From Nano to Macro, 2004, pp. 944–947.
[9]Cha, K. S., *et al*. Modeling the interaction of coils with the local blood flow after coil embolization of intracranial aneurysms. *J. Biomech. Eng*. 129(6):873–879, 2007.
[10]Fernandez, M. A., J.-F. Gerbeau, and V. Martin. Numerical simulation of blood flows through a porous interface. *ESAIM: Math. Model. Numer. Anal*. 42(2008):961–990, 2008.
[11]Humphrey, J. D. Cardiovascular Solid Mechanics: Cells, Tissues, and Organs. New York: Springer, 2002, 757 pp.
[12]Jou, L. D., D. Saloner, and R. T. Higashida. Determining intra-aneurysmal flow for coiled cerebral aneurysms with digital fluoroscopy. *Biomed. Eng. Appl. Basis Commun*. 16:43–48, 2004.
[13]Kakalis, N. M., *et al*. The haemodynamics of endovascular aneurysm treatment: a computational modelling approach for estimating the influence of multiple coil deployment. *IEEE Trans. Med. Imaging* 27(6):814–824, 2008.
[14]Kallmes, D. F., *et al*. A new endoluminal, flow-disrupting device for treatment of saccular aneurysms. *Stroke* 38(8): 2346–2352, 2007.
[15]Kim, S. H., *et al*. Endovascular treatment by using double stent method for ruptured vertebral artery dissecting aneurysms. *J. Korean Neurosurg. Soc*. 38:132–135, 2005.
[16]Kim, M., *et al*. Quantification of hemodynamic changes induced by virtual placement of multiple stents across a wide-necked basilar trunk aneurysm. *Neurosurgery* 61(6):1305–1312, 2007; discussion 1312–1313.
[17]Kim, M., *et al*. Comparison of two stents in modifying cerebral aneurysm hemodynamics. *Ann. Biomed. Eng*. 36(5): 726–741, 2008.
[18]Lieber, B. B., A. P. Stancampiano, and A. K. Wakhloo. Alteration of hemodynamics in aneurysm models by

stenting: influence of stent porosity. *Ann. Biomed. Eng.* 25(3):460–469, 1997.
[19]Meng, H., *et al.* A model system for mapping vascular responses to complex hemodynamics at arterial bifurcations in vivo. *Neurosurgery* 59(5):1094–1100, 2006; discussion 1100–1101.
[20]Meng, H., *et al.* Complex hemodynamics at the apex of an arterial bifurcation induces vascular remodeling resembling cerebral aneurysm initiation. *Stroke* 38(6):1924–1931, 2007.
[21]Mitsos, A. P., *et al.* Haemodynamic simulation of aneurysm coiling in an anatomically accurate computational fluid dynamics model: technical note. *Neuroradiology* 50(4): 341–347, 2008.
[22]Molyneux, A., *et al.* International Subarachnoid Aneurysm Trial (ISAT) of neurosurgical clipping versus endovascular coiling in 2143 patients with ruptured intracranial aneurysms: a randomised trial. *Lancet* 360(9342):1267–1274, 2002.
[23]Nguyen, T. N., *et al.* Comparison of ruptured vs unruptured aneurysms in recanalization after coil embolization. *Surg. Neurol.* 68(1):19–23, 2007.
[24]Radaelli, A. G., *et al.* Reproducibility of haemodynamical simulations in a subject-specific stented aneurysm model—a report on the Virtual Intracranial Stenting Challenge 2007. *J Biomech* 41(10):2069–2081, 2008.
[25]Reymond, P., *et al.* Validation of a one-dimensional model of the systemic arterial tree. *Am. J. Physiol. Heart Circ. Physiol.* 297(1):H208–H222, 2009.
[26]Sadasivan, C., *et al.* Treatment of rabbit elastase-induced aneurysm models by flow diverters: development of quantifiable indexes of device performance using digital subtraction angiography. *IEEE Trans. Med. Imaging* 28(7): 1117–1125, 2009.
[27]Schievink, W. I., *et al.* Intracranial aneurysm surgery in Ehlers-Danlos syndrome type IV. *Neurosurgery* 51(3): 607–611, 2002; discussion 611–613.
[28]Vernooij, M. W., *et al.* Incidental findings on brain MRI in the general population. *N. Engl. J. Med.* 357(18):1821–1828, 2007.
[29]Wailliez, C. and G. Coussement. CFD Study of Multilayer Stent Haemodynamics Effects in Abdominal Aortic Aneurysms. www.cardiatis.com.
[30]Wang, Z., *et al.* Molecular alterations associated with aneurysmal remodeling are localized in the high hemodynamic stress region of a created carotid bifurcation. *Neurosurgery* 65(1):169–177, 2009; discussion 177–178.
[31]Weir, B. K., *et al.* Cigarette smoking as a cause of aneurysmal subarachnoid hemorrhage and risk for vasospasm: a report of the Cooperative Aneurysm Study. *J. Neurosurg.* 89(3):405–411, 1998.
[32]Wiebers, D. O., *et al.* Unruptured intracranial aneurysms: natural history, clinical outcome, and risks of surgical and endovascular treatment. *Lancet* 362(9378):103–110, 2003.
[33]Zenteno, M. A., *et al.* Sole stenting bypass for the treatment of vertebral artery aneurysms: technical case report. *Neurosurgery* 57(1 Suppl):E208, 2005; discussion E208.